Reduced Field-of-View MRI Using Outer Volume Suppression for Spinal Cord Diffusion Imaging

B.J. Wilm,[1,2*] J. Svensson,[1,3] A. Henning,[2] K.P. Pruessmann,[2] P. Boesiger,[2] and S.S. Kollias[1]

A spin-echo single-shot echo-planar imaging (SS-EPI) technique with a reduced field of view (FOV) in the phase-encoding direction is presented that simultaneously reduces susceptibility effects and motion artifacts in diffusion-weighted (DW) imaging (DWI) of the spinal cord at a high field strength (3T). To minimize aliasing, an outer volume suppression (OVS) sequence was implemented. Effective fat suppression was achieved with the use of a slice-selection gradient-reversal technique. The OVS was optimized by numerical simulations with respect to T_1 relaxation times and B_1 variations. The optimized sequence was evaluated in vitro and in vivo. In simulations the optimized OVS showed suppression to <0.25% and ~3% in an optimal and worst-case scenario, respectively. In vitro measurements showed a mean residual signal of <0.95% ± 0.42 for all suppressed areas. In vivo acquisition with 0.9 × 1.05 mm^2 in-plane resolution resulted in artifact-free images. The short imaging time of this technique makes it promising for clinical studies. Magn Reson Med 57:625–630, 2007. © 2007 Wiley-Liss, Inc.

Key words: spinal cord; diffusion imaging; reduced FOV; outer volume suppression; DTI

In recent years diffusion tensor imaging (DTI) (1) of the brain has become feasible for investigating various neurological pathologies that affect the human brain. This method has not yet found its way into clinical applications involving the spinal cord; however, it is expected to improve our understanding of the nature and evolution of structural damage in several clinical conditions, such as trauma, inflammatory demyelination, and tumors.

In the brain the most established approach for acquiring diffusion-weighted (DW) images is single-shot echo-planar imaging (SS-EPI). This technique benefits from being more robust against ghosting artifacts due to physiological motion, and from a relatively high signal-to-noise ratio (SNR), which can be further improved by acquisition at higher field strength (3T).

In the spinal cord SS-EPI suffers from strong susceptibility gradients induced by the surrounding tissues, particularly the osseous elements of the spinal column. This problem increases at 3T, and the readout train for a conventional SS-EPI acquisition with sufficient resolution to image the spinal cord will be too long to yield images of adequate quality.

Although several approaches to overcome these problems have been tested, it remains difficult to achieve stable, high-resolution DW acquisitions in the spinal cord. An excellent introduction to this topic can be found in Ref. 2.

The morphology of the spinal cord, particularly its small cross-sectional dimensions, allows the use of a reduced-FOV approach (3,4), with a rectangular FOV centered on the region of interest (ROI). The corresponding reduction of the required number of *k*-space lines enables SS-EPI to be performed with a shorter readout duration, leading to a reduction in susceptibility artifacts. However, to prevent aliasing artifacts, the acquisition of signal from the region outside the FOV (i.e., the outer volume (OV)) must be avoided.

The aim of this study was to develop a technique for DW imaging (DWI)/DTI of the cervical spinal cord in the transversal plane that is insensitive to susceptibility and motion artifacts, and can be performed within clinically relevant scan times. In the reduced-FOV, SS-EPI approach presented here, we address the problem of signal aliasing by suppressing the OV with specifically designed presaturation slabs. An OV suppression (OVS) sequence (5) was optimized for application to the cervical spinal cord. Additionally, a spin-echo fat suppression by gradient reversal technique (6) was implemented to avoid water–fat-shift artifacts. The performance of the suggested technique was evaluated in in vitro and in vivo scans.

THEORY

OVS

OVS utilizes one or more spatially selective pulses applied in the OV regions followed by dephasing gradients. The OVS sequence is placed before the slice excitation pulse of the imaging sequence. Effective OVS requires complete dephasing of the transverse magnetization and nulling of all longitudinal magnetization at the time of the excitation pulse. In the present case the regions on both sides of the spinal cord have to be suppressed. Hence, separate OVS pulses must be applied on the left and right sides of the FOV in the phase direction. In the absence of transversal magnetization, the longitudinal magnetization at a time τ_i after the i_{th} pulse in a pulse train may be calculated according to:

$$M_i = M_{i-1}e^{-(\tau_i/T_1)}\cos(\alpha_i) + M_0(1 - e^{-(\tau_i/T_1)})$$

Where M_{i-1} is the longitudinal magnetization just before application of the i_{th} pulse, α_i is the flip angle of the i_{th} pulse, and M_0 is the equilibrium magnetization.

[1]Institute of Neuroradiology, University Hospital Zurich, Zurich, Switzerland.
[2]Institute of Biomedical Engineering, University and ETH Zurich, Zurich, Switzerland.
[3]Department of Radiation Physics, Malmö University Hospital, Lund University, Malmö, Sweden.

Grant sponsor: Swiss National Science Foundation.

*Correspondence to: Bertram Wilm, Institute for Biomedical Engineering, University and ETH Zurich, Gloriastrasse 35, CH-8092 Zurich, Switzerland. E-mail: wilm@biomed.ee.ethz.ch

Received 21 June 2006; revised 17 November 2006; accepted 20 November 2006.
DOI 10.1002/mrm.21167
Published online in Wiley InterScience (www.interscience.wiley.com).

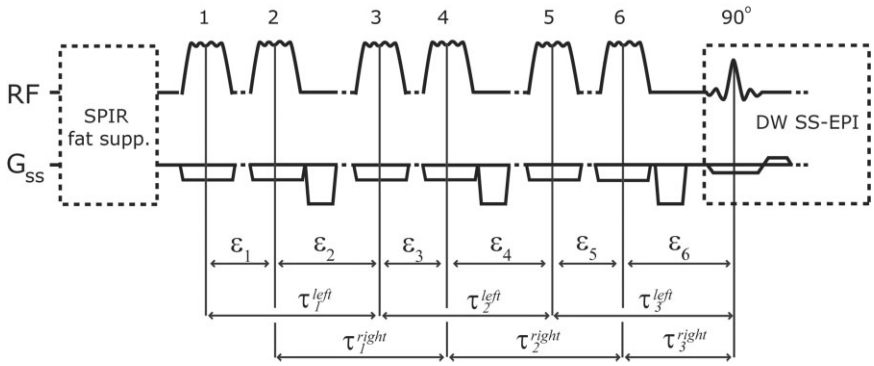

FIG. 1. Schematic representation of the DW SS-EPI sequence preceded by the presaturation OVS sequence and the SPIR pulse. Each pair of quadratic-phase pulses (first pulse for the left slab, and second pulse for the right slab) is followed by crusher gradients. ϵ_i denotes the interval between the center of the i^{th} and the center of the following pulse, and τ_i is the time between two consecutive pulses applied in the same geometric region. G_{ss} denotes the gradient in the slice-selection direction.

The design of a sequence that accomplishes effective OVS requires optimization of several parameters. Since the presaturation slabs should be highly selective, the use of broad-banded pulses to excite a well-defined spatially broad region (here 60 mm) even in regions of inhomogeneous B_0 is desirable. For this reason we chose to use quadratic-phase Shinnar-Le Roux pulses (7,8). The fractional transition width (FTW), which is defined by the transition width (TW)/bandwidth (BW), was fixed such that the transition band had a spatial width of 4 mm, and all pulses had a minimum BW of 4700 Hz. Thus the pulse durations dur_i were fixed for each flip angle α.

By using multiple applications of suppression pulses, one can enhance the T_1 insensitivity and/or B_1 insensitivity of the OVS. For each saturation region (left and right) we used three pulses, which still allowed the acquisition of one slice per cardiac cycle without violating specific absorption rate (SAR) limitations. To keep the OVS applicable for arbitrary interacquisition delays (which may change according to the number of slices acquired during each TR, or by varying cardiac frequencies for cardiac-triggered acquisitions), the first two flip angles for each slab were fixed at 90°. This achieves a B_1-insensitive nulling of all initial longitudinal magnetization of any OV tissue in the first part of the OVS sequence. The six pulses were fixed to affect the left and right OVs in an alternating manner to minimize the number of required crusher gradients (Fig. 1). The interpulse timings ϵ were fixed to the shortest practical value (while still nulling longitudinal magnetization at excitation time) to improve T_1 insensitivity and decrease the total time of the OVS sequence.

A schematic representation of the presaturation pulse sequence is given in Fig. 1.

Fat Suppression

Fat suppression is usually implemented by a spectral inversion recovery (SPIR) pulse preceding the slice-selection pulse, which makes it necessary to place the SPIR pulse before the OVS. Due to the application of the OVS pulses, the fat suppression in the transition bands of the pulses will be unsatisfactory, resulting in fat-shift artifacts. Therefore, in addition to the SPIR pulse preceding the OVS, we implemented a reverse-gradient technique (6) using a small BW ($\leq$572 Hz) for excitation and echo pulse.

To avoid unwanted signal rephasing, all gradients on the slice-selection axis preceding the excitation pulse were assigned the same sign as the slice-selection gradient (Fig. 1).

MATERIALS AND METHODS

OVS Optimization

Numerical optimization of the OVS for the free parameters (i.e., the third flip angle α_3 and the interpulse durations ϵ_i; see Fig. 1) was performed on a personal computer with the use of Matlab 7.0.1 (The MathWorks, Inc., Natick, MA, USA). The simulation minimized longitudinal magnetization at the time of the excitation pulse for tissues with T_1's of 292 ms and 1160 ms (approximate relaxation times at 3T for fat and skeletal muscle) for the left and right OVs, respectively.

Pulse intervals ϵ_i were constrained by the pulse durations and by the time required for dephasing gradients and eddy-current decay periods. For the optimized parameter configuration, residual longitudinal magnetizations were calculated for a range of T_1 (280–1500 ms), which covers the range of in vivo tissue. To account for the frequency sweep (7,9) of the quadratic-phase pulses, timing offsets of up to $\pm dur/2$ of the pulses nominal application time were incorporated into the calculations. Flip angle variations due to B_1 inhomogeneities of –20% to +5% (according to Ref. 10 for the in vivo variation of the B_1 field) were also incorporated. The sequence that resulted in a minimal maximum residual longitudinal magnetization over the whole range of T_1 was chosen as the optimum sequence.

Experimental Setup

All imaging was performed on a 3T Philips Achieva MR system (Philips Medical Systems, Best, The Netherlands) using a 12-element phased-array spinal coil.

In Vitro

The optimized OVS sequence obtained with the numerical simulation was tested in vitro and evaluated for its efficacy of suppression and for effects that had been neglected by the simulations, such as excitation profiles and the generation of spurious echoes.

To simulate in vivo behavior of skeletal muscle and fat tissue in a phantom, liquids with corresponding T_1 relaxation constants (distilled water doped with gadolinium to $T_1 \approx 1160$ ms, and vegetable oil with $T_1 \approx 290$ ms) were placed into a bottle. To evaluate residual signal from the suppressed areas, the phantom was scanned on a full FOV with a T_2-weighted (T_2W) multishot EPI sequence to avoid susceptibility artifacts. The full FOV covered the entire

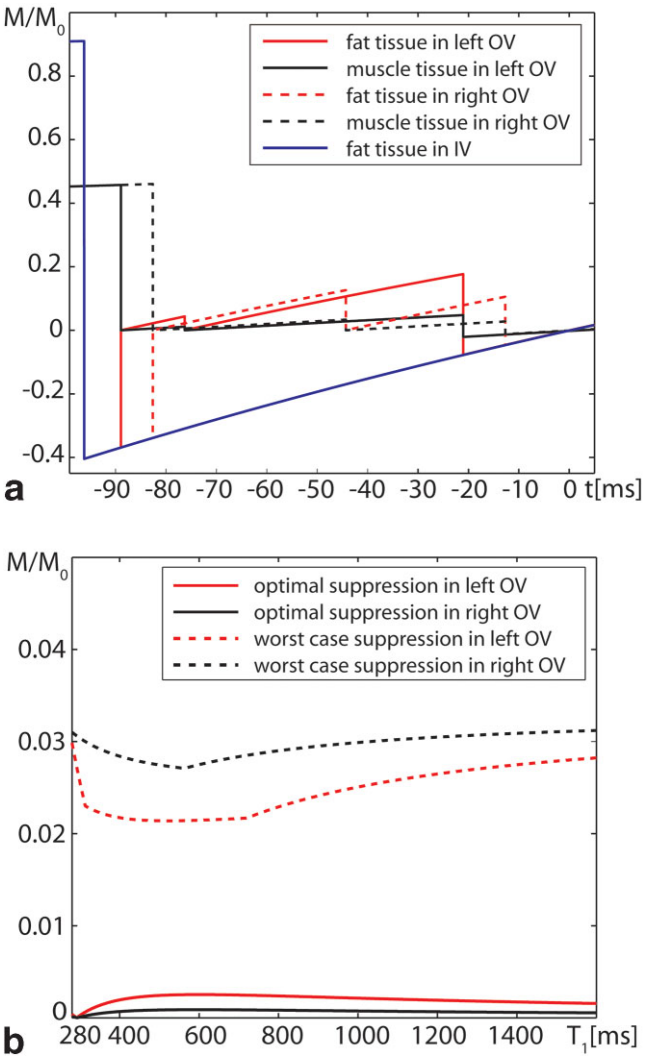

FIG. 2. **a:** Simulated longitudinal magnetization in the different tissue compartments over the time course of the application of the optimized OVS sequence, neglecting T_1 and timing offsets. **b:** Residual longitudinal magnetization M/M_0 in the left and right OVs vs. T_1 for the optimized OVS simulated without (optimal) and with (worst case) the effect of maximal B_1 variations and timing offsets.

phantom in the axial plane with the two suppression slabs (slab width = 60 mm each) applied on the left and right parts of the image while the middle portion of the image was left unsuppressed. The scan parameters were FOV = 130 × 130 mm^2, matrix = 144 × 144, TR = 3000 ms, TE = 40 ms, slice thickness = 5 mm, and signal averages = 10. An EPI factor of 15 was used to avoid susceptibility effects and to create a clearly visible fat shift of 11.4 pixels in the anterior direction to separate lipid and nonlipid spins in the oil compartment of the phantom.

Two sets of images were acquired: one with OVS and fat suppression, and one without. The efficacy of the suppression (defined as the fraction of suppressed to unsuppressed signal) was measured in different regions of interest (ROIs) placed in each of these image pairs. To illustrate the effect of the different methods combined in this approach, images with OVS but without fat suppression, and images with OVS and SPIR fat suppression only were also acquired.

In Vivo

In vivo 2D spin-echo SS-EPI DTI data of the cervical spinal cord were acquired between levels C-3 and C-5 in five healthy subjects. Images were acquired in axial orientation using the optimized OVS sequence.

Acquisition (slice thickness = 5 mm, NEX = 6/12 for $b = 0/b = 750$ s/mm^2, matrix = 144 × 32, FOV = 130 × 32.5 mm^2, TR = 3500 ms, TE = 40.6 ms) was carried out along six noncollinear diffusion directions. Additionally, for each slice a baseline image with minimal diffusion weighting (B_0 image) was acquired. The shortest possible readout train duration was chosen and further shortened by a partial Fourier encoding of 0.6 to limit T_2 decay and phase effects from susceptibility gradients. The phase-encoding direction was set left–right (LR) to avoid high signal foldover originating from tissue near the coil surface. The EPI readout time was reduced from 111 to 28 ms, as compared to a full-FOV matrix size of 144 × 144. The scan time was 48 s per slice for a multislice setup due to SAR restrictions.

To correct for interscan motion and eddy-current-induced distortions, the data sets were coregistered (11). Subsequently, the mean apparent diffusion coefficient (ADC), relative anisotropy (RA), and fractional anisotropy (FA) (12) were calculated for each data set. ROIs covering the gray matter (GM) and white matter (WM), respectively, were carefully placed in each slice after close consideration of the anisotropy, DW, and T_2W images.

RESULTS

Simulation

For each maximum flip angle α, the numerical optimization returned the interpulse timings ϵ to achieve a theoretical nulling of the longitudinal magnetizations M_z in all compartments at excitation time, which is displayed for the finally chosen parameter constellation in Fig. 2a. When timing variations due to the frequency sweep and flip angle variations were taken into account, optimal suppression was found for a flip angle of 116°. The parameters of this optimized OVS sequence are given in Table 1. Even when we assumed maximum flip angle variations and timing offsets (termed "worst-case suppression" in Fig. 2b), the residual longitudinal magnetization was no more than approximately 3% for the whole range of tissue T_1. The difference in efficacy of suppression in the left and right OVs results from timing differences of the OVS pulses.

Table 1
The Optimized Configuration for the OVS Sequence

i	1	2	3	4	5	6
ϵ_i (ms)	6.5	8.6	33.1	24.0	8.7	13.23
α_i	90	90	90	90	116	116
dur_i (ms)	6.	6.5	6.5	6.5	8.7	8.7

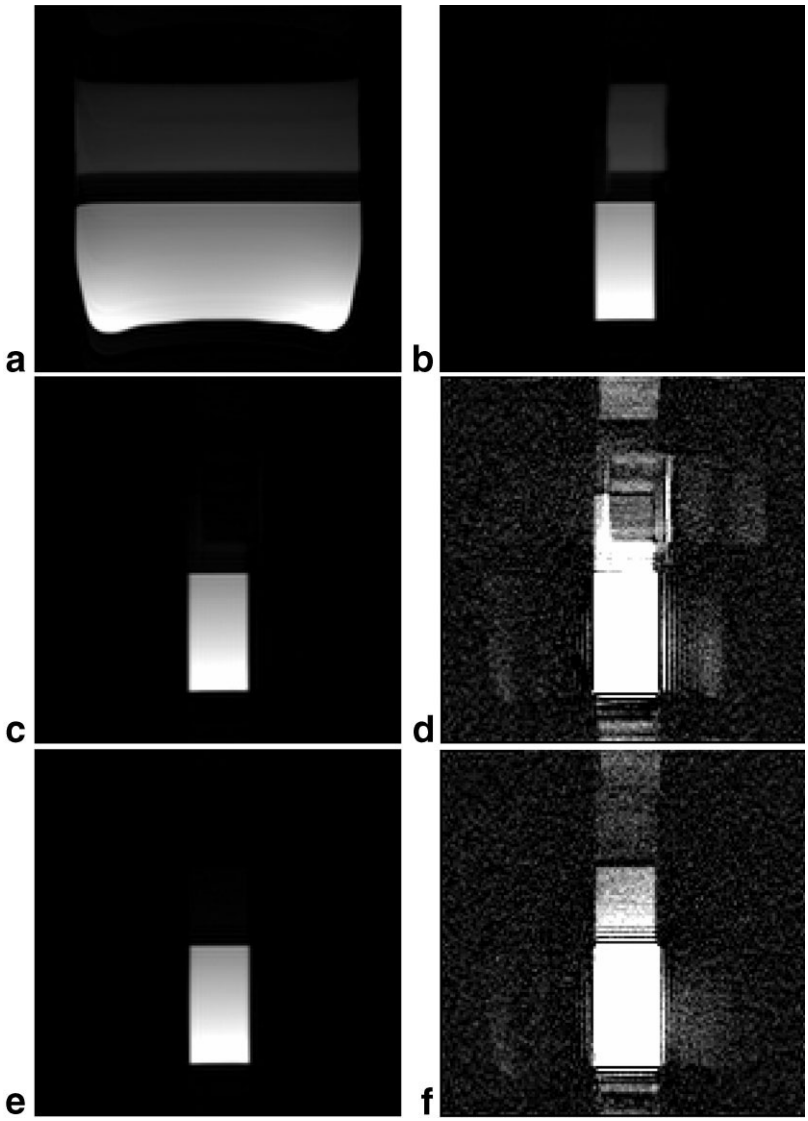

FIG. 3. SS-EPI images of a phantom with water (below) and oil (above) with its lipid section shifting to anterior: (**a**) without OVS or fat suppression, (**b**) with OVS but without fat suppression, (**c** and **d**) with OVS and SPIR fat suppression, and (**e** and **f**) with OVS, SPIR fat suppression, and gradient-reversal fat suppression. d,f: Show the same data as c and e, respectively, with the window set to display noise level. d: Displays the residual inner volume fat shifting in upper-right direction (readout and slab-selection fat shift) with hyperintense signal in the TW of the suppression pulses. f: Shows complete suppression of all lipid signal. Only the inner volume water-spins exhibit signal.

In Vitro Scans

Figure 3 demonstrates the effect of the different modules of the sequence on the suppression profiles. The residual signal, measured in the different ROIs from repeated multishot EPI measurements (Fig. 3a and e), was approximately 1% in the "muscular" compartments (T_1 = 1160 ms). For the inner volume (IV) and OV lipid compartments the residual signal was below the noise level (not measurable) despite their high SNR (~190) in the unsuppressed images. Suppression profiles were well defined, and no artifacts from spurious echoes were visible in any acquired data set (Fig. 3b–f).

In Vivo Scans

Figure 4a shows the obtained images in the contrasts T_2, mean DW, mean ADC, and RA. To illustrate the robustness of our method, the center image of the imaging stack for each subject is shown in the mean DW and RA contrast (Fig. 4). No susceptibility, motion, or water–fat-shift artifacts were observed in any of the acquired data sets. Foldover artifacts (indicated by structured hyper- or hypointensities not in accordance with anatomical structures) were absent on both DW and T_2W images. In particular, the hypointense CSF in the DW images did not show any local hyperintensities in any of the acquired slices (Fig. 4).

The GM was depicted slightly hyperintense compared to the WM on T_2W and mean DW images. GM-WM contrast was better displayed in the anisotropy images, with the WM appearing hyperintense due to its high content in myelinated fibers. Nerve roots were best visible on the mean DW images (Fig. 4a and b), but were only faintly visible in all other contrasts. The measured quantitative diffusivity values averaged over all subjects are given in Table 2.

DISCUSSION

We have introduced a reduced-FOV approach for spinal cord diffusion imaging in the transverse plane at 3T. The resulting reduction in the required number of *k*-space lines

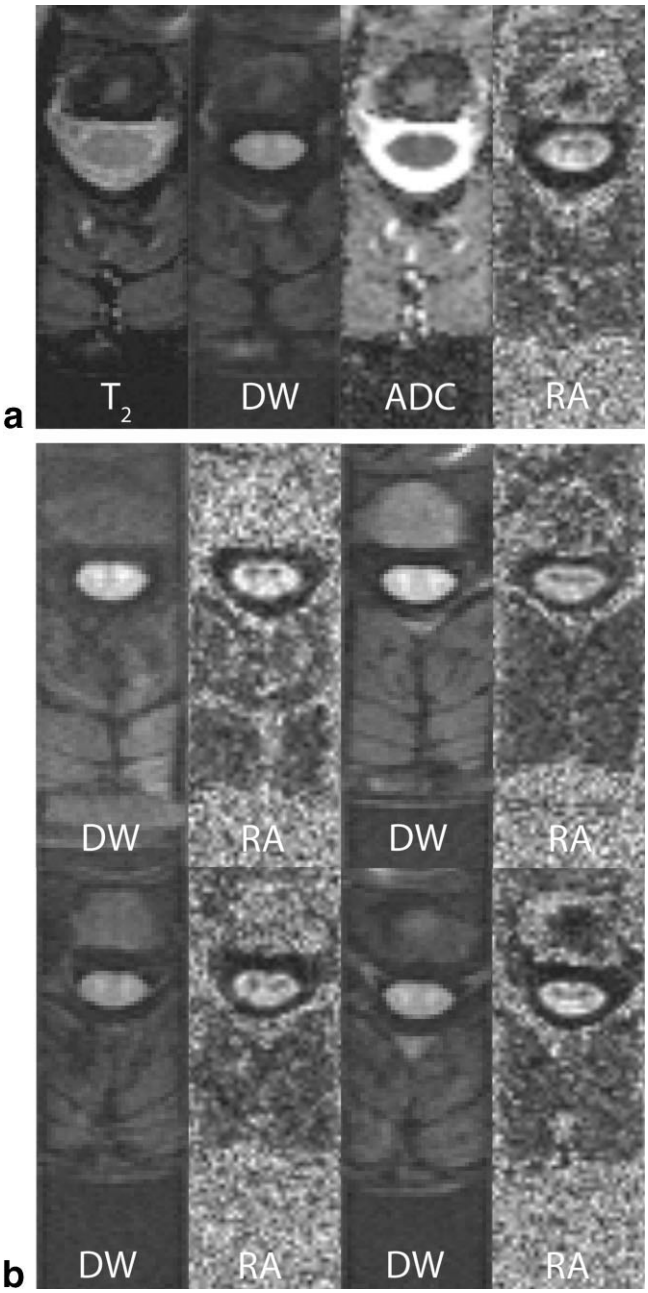

FIG. 4. Transversal slice of the spinal cord at approximately level C-4 (center slice of imaging stack) in different contrasts. **a:** Subject 1: T_2, mean DW, mean ADC, and RA. **b:** Subjects 2–5: mean DW and RA.

makes it possible to achieve high-resolution SS-EPI acquisitions without susceptibility or motion artifacts. Foldover artifacts are efficiently avoided by optimizing the OVS in terms of B_0, B_1, and T_1 insensitivity.

The gradient-reverse fat-suppression technique proved to be efficient at avoiding spin echoes from lipid compartments without the cost of an extra RF deposit. Depending on the required BW of the spin-echo pulses, this T_1-insensitive fat-suppression technique may be employed in the future without SPIR even at 3T.

The fact that the anisotropy contrast does not display the expected butterfly shape of the GM consistently in all images may be attributed to the relatively low SNR, partial-volume effects, and possibly also to imprecise coregistration. These factors may also explain why the measured FA values were higher than the previously reported values of FA(WM) = 0.65, FA(GM) = 0.34 (13), and the contrast in mean ADC was less discriminative than that reported in Ref. 2 (mean ADC(WM) = 0.77–0.80; mean ADC(GM) = 1.0–1.1 10^{-3}mm^2/s. To our knowledge, these are the only published data that distinguish the diffusivity values of GM and WM. The in-plane resolution of 0.9 mm × 1.05 mm for axial DWI of the spinal cord was similar to that reported in other studies (1.25 mm × 1.25 mm (4,13), and 0.96 mm (14)).

The presented methods were integrated into the software of our clinical MR system. Hence, OVS and the reverse fat-suppression technique can be combined with the existing sequences via the user interface without further modifications or preparations. Similarly to parallel imaging, this approach enables TE shortening and less T_2* blurring, but is naturally immune to sensitivity miscalibration. Furthermore, for the same reduction of sampled *k*-space lines, the images produced by parallel imaging will have a lower SNR by a factor of $1/g$ (where g is the geometry factor) (15). Compared to zonally magnified oblique multislice echo planar imaging (ZOOM-EPI) (4), our approach provides a more effective readout time reduction due to the well-defined rectangular signal profile. Furthermore, multislice acquisition does not require the slice stack to be split into multiple packages, which, depending on the geometry used, may prolong the scan time. In contrast to the reduced-FOV approach (3), multislice imaging with our method will not result in signal loss. However, the acquisition speed of our method is limited by SAR constraints to one slice acquisition every 750 ms. Both of the above-mentioned reduced-FOV approaches are limited to spin-echo acquisitions, whereas the proposed approach may also be combined with gradient-echo techniques for other applications.

The application of this technique in other regions of the spinal cord is desirable, but is currently limited by the BW and residual OV signal from multiple foldover.

CONCLUSIONS

We have introduced OVS for reduced-FOV SS-EPI spinal cord diffusion imaging in the axial orientation. Reducing the FOV enabled high-resolution acquisition of the cervical spinal cord without visible susceptibility or motion artifacts. Water–fat-shift artifacts were successfully avoided with the use of SPIR together with a spin-echo gradient-reversal technique. The virtually artifact-free im-

Table 2
Measured Quantitative Diffusivity Values Averaged Over All Five Subjects (ROI Sizes: GM = ~80 Voxels/Subject; WM = ~ 170 Voxels/Subject).

ROI	FA (μ,σ)	RA (μ,σ)	Mean ADC (μ,σ) [10^{-3}mm^2/s]
GM	0.56 ± 0.14	0.53 ± 0.15	0.94 ± 0.14
WM	0.76 ± 0.10	0.81 ± 0.15	0.97 ± 0.15

ages and the short imaging time make this method promising for clinical applications of diffusion imaging in the human cervical spinal cord.

ACKNOWLEDGMENTS

The authors thank Thomas Lange for fruitful discussions, and Kai Eberhardt for reviewing the manuscript.

REFERENCES

1. Basser PJ, Mattiello J, LeBihan D. MR diffusion tensor spectroscopy and imaging. Biophys J 1994;66:259–267.
2. Bammer R, Fazekas F. Diffusion imaging of the human spinal cord and the vertebral column. Top Magn Reson Imaging 2003;14:461–476.
3. Jeong EK, Kim SE, Guo J, Kholmovski EG, Parker DL. High-resolution DTI with 2D interleaved multislice reduced FOV single-shot diffusion-weighted EPI (2D ss-rFOV-DWEPI). Magn Reson Med 2005;54:1575–1579.
4. Wheeler-Kingshott CAM, Hickman SJ, Parker GJM, Ciccarelli O, Symms MR, Miller DH, Barker GJ. Investigating cervical spinal cord structure using axial diffusion tensor imaging. Neuroimage 2002;16:93–102.
5. Ogg RJ, Kingsley PB, Taylor JS. WET, a T1- and B1-insensitive water-suppression method for in vivo localized 1H NMR spectroscopy. J Magn Reson B 1994;104:1–10.
6. Volk A, Tiffon B, Mispelter J, Lhoste JM. Chemical shift-specific slice selection—a new method for chemical-shift imaging at high magnetic-field. J Magn Reson 1987;71:168–174.
7. Schulte RF, Tsao J, Boesiger P, Pruessmann KP. Equi-ripple design of quadratic-phase RF pulses. J Magn Reson 2004;166:111–122.
8. Le Roux PH, Gilles RJ, McKinnon GC, Carlier PG. Optimized outer volume suppression for single-shot fast spin-echo cardiac imaging. J Magn Reson Imaging 1998;8:1022–1032.
9. Garwood M, DelaBarre L. The return of the frequency sweep: designing adiabatic pulses for contemporary NMR. J Magn Reson 2001;153:155–177.
10. Treier R, Steingoetter A, Fried M, Schwizer W, Boesiger P. On the necessity of flip angle correction for fast T1 mapping using DESPOT 1. In: Proceedings of the 14th Annual Meeting of ISMRM, Seattle, WA, USA, 2006 (Abstract 2264).
11. Netsch T, Muiswinkel AV. Quantitative evaluation of image-based distortion correction in diffusion tensor imaging. IEEE Trans Med Imaging 2004;23:789–798.
12. Basser PJ. Inferring microstructural features and the physiological state of tissues from diffusion-weighted images. NMR Biomed 1995;8:333–344.
13. Maier SE, Mamata H. Diffusion tensor imaging of the spinal cord. Ann NY Acad Sci 2005;1064:50–60.
14. Wilson GJ, Wang P, Szumowski J, Hoogenrad FG. Diffusion-weighted imaging of the spinal cord using SENSE at 3T. In: Proceedings of the 12th Annual Meeting of ISMRM, Kyoto, Japan, 2004 (Abstract 11).
15. Pruessmann KP, Weiger M, Scheidegger MB, Boesiger P. SENSE: sensitivity encoding for fast MRI. Magn Reson Med 1999;42:952–962.